Smart Structures and Systems, *Vol. 19, No. 6 (2017) 679-694*
DOI: https://doi.org/10.12989/sss.2017.19.6.679

Dynamic torsional response measurement model using motion capture system

Hyo Seon Park[1], Doyoung Kim[1], Su Ah Lim[1] and Byung Kwan Oh[*2]

[1]*Department of Architectural Engineering, Yonsei University, Seoul 120-749, Republic of Korea*
[2]*Center for Structural Health Care Technology in Building, Yonsei University, Seoul 120-749, Republic of Korea*

(Received November 2, 2016, Revised April 20, 2017, Accepted May 7, 2017)

Abstract. The complexity, enlargement and irregularity of structures and multi-directional dynamic loads acting on the structures can lead to unexpected structural behavior, such as torsion. Continuous torsion of the structure causes unexpected changes in the structure's stress distribution, reduces the performance of the structural members, and shortens the structure's lifespan. Therefore, a method of monitoring the torsional behavior is required to ensure structural safety. Structural torsion typically occurs accompanied by displacement, but no model has yet been developed to measure this type of structural response. This research proposes a model for measuring dynamic torsional response of structure accompanied by displacement and for identifying the torsional modal parameter using vision-based displacement measurement equipment, a motion capture system (MCS). In the present model, dynamic torsional responses including pure rotation and translation displacements are measured and used to calculate the torsional angle and displacements. To apply the proposed model, vibration tests for a shear-type structure were performed. The torsional responses were obtained from measured dynamic displacements. The torsional angle and displacements obtained by the proposed model using MCS were compared with the torsional response measured using laser displacement sensors (LDSs), which have been widely used for displacement measurement. In addition, torsional modal parameters were obtained using the dynamic torsional angle and displacements obtained from the tests.

Keywords: structural health monitoring; dynamic torsional displacement; motion capture system

1. Introduction

There have been a number of researches on structural health monitoring (SHM) to evaluate the condition of structures and assess their safety in the fields of mechanical, civil, and architectural engineering (Ansari 1997, Frangopol *et al*. 2008, Park *et al*. 2008, Jang *et al*. 2010, Ni *et al*. 2012). In these studies, responses measured from sensors installed in the structure are used to evaluate the safety of structural elements within the structure. In addition, from the responses, system identification to find modal parameters is performed to evaluate condition of structure in the system level. However, the complexity, enlargement and atypia of a structure lead to an increase in the irregularity and asymmetry of stiffness in the vertical and horizontal directions of the structure. Furthermore, uncertain dynamic loads that act on a structure are not uni-directional but multi-directional. Therefore, such discontinuous structural stiffness caused by structure's shape and uncertain load conditions create complex load transfer mechanisms; as a result, unexpected structural behavior, such as torsion, occurs. Continuous torsion, which occurs throughout the structure, causes an undesired stress in the local structural members, resulting in a reduction of the structural performance and the structure's lifespan. Therefore, torsion monitoring technology is required to ensure the safety of structures and minimize the structural damage and the economic and human injuries caused by the torsional behaviors of structures.

In the previous researches on the monitoring of the torsion of structures, the structure's dynamic properties were obtained mainly from vibration measurements and were used to identify state of the structure and to detect and evaluate damage (Yacamini *et al*. 1998, Duffey *et al*. 2001, Yoshida *et al*. 2003, Im *et al*. 2013). Researches have also focused on monitoring structural torsion by directly measuring the torsion angle of a structure, rather than obtaining torsion modal properties through vibration measurements. Fiber Bragg grating (FBG) sensors have been used to measure a structure's tilt angle and temperature (Yang *et al*. 2015), the torsional angle has been measured at the structural member level (Zhang *et al*. 2002), photonic crystal fibers have been used to measure the torsional angle and direction simultaneously (Chen *et al*. 2014), and a torsional angle measurement model has been developed based on a dual polarized Mach-Zehnder interface (Chen *et al*. 2011). Although those methods can measure the angle of torsion occurring within a structural member locally, it is difficult for them to measure the torsion that occurs throughout the structure in the system level. In addition, torsion that occurs in a structure by an external load is accompanied by translational and rotational displacement, and a method for simultaneously measuring those responses is required.

The torsional responses are divided into pure rotation

*Corresponding author, Ph.D.
E-mail: aeioobk@yonsei.ac.kr

http://www.techno-press.com/journals/sss&subpage=8
ISSN: 1738-1584 (Print), 1738-1991 (Online)

and translation displacement. Pure rotation and translation displacement are used to calculate the torsional angle and displacement, respectively. The torsional displacement will be represented as the pure translation displacement extracted by removing pure rotation component in the torsional response in this paper. To measure those torsional responses including translation displacement, a method estimating torsional responses using a displacement measurement can be considered as a candidate sensing approach for torsion monitoring. The linear variable differential transformer (LVDT) and laser displacement sensor (LDS) (Park *et al*. 2013, Keyence Co. 2016) have been widely used for measuring displacement. To measure the structure's movement, these sensors are attached to the structure and detect displacement changes in the structural movement with relatively high precision, but only under the condition that the contact part of the sensor and the installation place are stable. Furthermore, installation is restrictive because the sensor must be installed at a reference point that is not influenced by the target's behavior. Because most of the fields where structures are constructed have many uncertain environmental variables, SHMs of torsion based on these sensors have practical limitations.

The global positioning system (GPS) (Juang 2000, Casciati and Fuggini 2011, Yi *et al*. 2013) is one of the non-contact displacement measurement sensors used in SHM. With GPS, real-time and long-term measurements are possible. In addition, GPSs are widely used in the monitoring of a variety of structures such as civil infrastructure and tall buildings. Lovse *et al*. (1995) monitored the dynamic deflection of the Calgary Tower in Alberta, Canada using GPS. Park *et al*. (2008) measured the displacements in a high-rise building during typhoons with GPS and Choi *et al*. (2013) evaluated stiffness change of high-rise building using GPS. Various researches (Roberts *et al.* 1999, Celebi and Sanli 2002, Roberts *et al*. 2004, Chan *et al*. 2006) used GPS to monitor high-rise buildings and bridges in real time. However, the measurements by GPS can be limited if there are tall buildings that block radio waves near the device. In addition, measurements using GPS are only possible outdoors such as the roof of a building. Further, the precision level of GPS is ±10 mm for horizontal directions and ±20 mm for vertical directions (Breuer *et al*. 2002), which impose limitations on the precision of torsional measurements.

Other methods for measuring displacement with non-contact sensors use technologies from the field of image-based photogrammetry. Among those methods, the digital image correlation (DIC) method (Lava *et al*. 2010) has been employed to measure deformations of a target using a charged coupled device (CCD) camera (Olaszek 1999, Fraser and Riedel 2000). A CCD camera requires precise measurement of the distance between the CCD camera and the reflection target point that is fixed on the structure. The camera's small measurement range and low sampling rate make it difficult to measure the dynamic behavior of a target. A motion capture system (MCS), one of the technologies from the field of image-based measurement, was introduced to measure dynamic displacements of a target structure in three-dimensional coordinates with high precision and at a high sampling rate. Researches have been conducted on using MCS to perform precise measurements of the dynamic displacement in a steel frame structure (Park *et al*. 2015a, Oh *et al*. 2015). In particular, MCS has been regarded to be appropriate to measure dynamic motions more precisely when a structure vibrates with translational and torsional deformations simultaneously compared with LDS only measuring one-dimensional displacement.

Although the displacement measurement equipment used in the previous researches can achieve precise displacement measurements within the range of acceptable error, no model has been developed on measuring or estimating torsional responses, including the torsional angle and displacements. This paper presents a model for measuring the dynamic torsional responses that accompanies torsional angle and displacement by using the dynamic displacement measured using a MCS. The model presented in this paper measures the dynamic torsional angle and displacements with the movements of two MCS markers on a plane of the structure. Vibration tests were performed to verify the applicability of the proposed model. The measured dynamic displacements were applied to the proposed model, the torsion angle and displacement were measured, and the results were compared with the values obtained using an existing displacement sensing method. The modal parameters, such as natural frequency and mode shapes for the torsional modes were found via system identification using the obtained dynamic torsion responses.

2. Principle of motion capture system

The MCS used in this paper refers to a technology that digitally records the positions of objects in a 3D space. Recently, it has been used in many fields beyond movies, such as medicine, sports, and robotics. The types of motion capture can be broadly divided into acoustic, mechanical, magnetic, and optical. The optical method uses an infrared camera to recognize an optical sensor, reflective marker attached to a person or an object, and depending on how the camera recognizes the marker, it is classified as a passive marker method or an active marker method. When perform measurement using the passive marker, the marker position is recognized by the reflection of light emitted from a camera strobe, and using the active marker, the marker itself emits light. In this research the vibration tests were performed using the passive marker of optical motion capture, and the markers were attached to the structure to measure the position of the structure in real time (NaturalPoint, Inc. DBA OptiTrack, Vicon Motion Systems Ltd). As shown in Fig. 1, the MCS consists of cameras, a computer, a server, and passive markers. Markers are attached to the places where the structure needs to be measured, and the camera positions are adjusted so that all of the markers are placed in camera’s angles of view in the test. The cameras are equipped with strobes that emit light. The light is reflected off the marker, and the camera measures the marker's movement. The data measured from the cameras are collected by the server and transmitted to the computer. At this time, each camera recognizes the coordinates of the markers attached to the structure as 2D coordinates. To obtain 3D coordinates, two or more cameras must be used. A T-shaped wand must be used for calibration to create (*X*, *Y*, *Z*) virtual standard coordinates as shown in Fig. 1. The data from this process are converted to 3D data. The converted 3D coordinates create the X, Y, and Z axes based on the wand coordinates, so they must be matched to the coordinate axes (*x*, *y*, z) based on the structure. Therefore, an Euler angle rotation matrix calculation method is used to convert the data based on wand coordinate axes to data based on structure coordinate axes (Park *et al*. 2015b). The details for Euler rotation method is presented in Appendix A. The raw data from rotation-converted data are filtered to produce the final measurement data. The filtered data are coordinate data from the structure coordinates, which can be used to observe the position information of each marker according to time.

3. Dynamic torsional response measurement model

3.1 Torsional angle measurement model

Structure’s torsional responses include the torsional angle and displacement which generally refer to pure rotational and translational displacements. Torsion reflects the structure's rotational behavior, so it can be quantified via the rotation angle. To measure the angle, one measurement point to act as a reference and one more measurement point that can reflect the amount of movement caused by rotation are needed. To measure both the torsional angle and displacement, at least two measurement points are needed. In other words, the structure's translational and rotational displacement cannot be distinguished and measured through the displacement of a single measurement point. To measure the torsion of a 2D plane with MCS, the rotational and translational displacement must be distinguished; therefore a minimum of two markers must be attached to the same plane (X-Y plane) of the structure. Markers can be attached to random locations on the same plane, and the dynamic torsional angle can be calculated through measurements, as shown in Fig. 2.

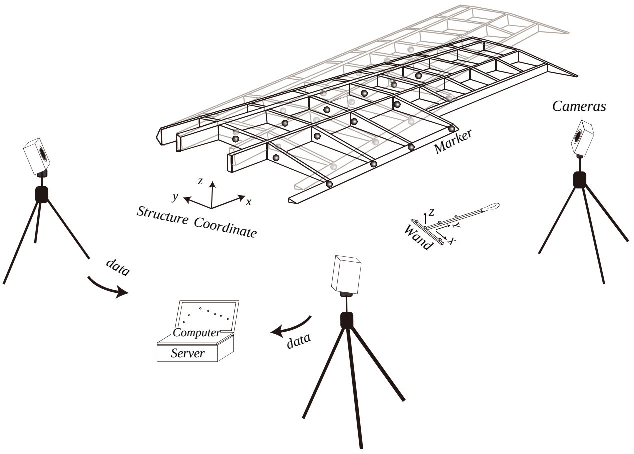

Fig. 1 MCS layout

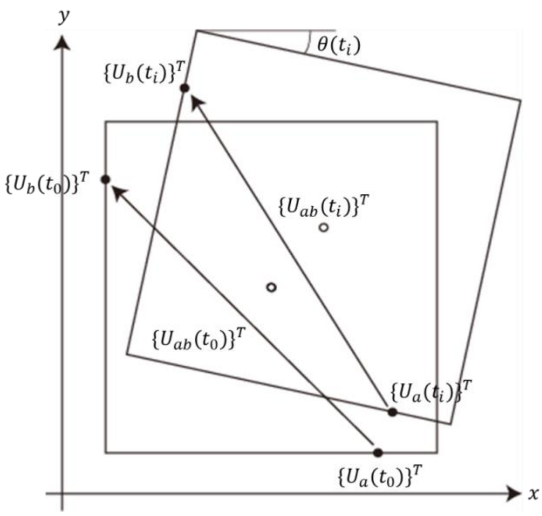

Fig. 2 Marker coordinate for torsional angle measurement

In Fig. 2, the 2D coordinates of markers (a) and (b) at random locations on the same plane are given as

$$\{U_a(t_i)\}^T = \begin{Bmatrix} x_a(t_i) \\ y_a(t_i) \end{Bmatrix}^T \qquad \{U_b(t_i)\}^T = \begin{Bmatrix} x_b(t_i) \\ y_b(t_i) \end{Bmatrix}^T \tag{1}$$

where t_i is the *i*-th measured time, and when $i = 0$, it indicates the time of the initial state. $U_a(t_i)$ is the 2D plane coordinates of marker (a). $x_a(t_i)$ is the X coordinate of marker (a), and $y_a(t_i)$ is the Y coordinate of marker (a). Similarly, $U_b(t_i)$, $x_b(t_i)$, and $y_b(t_i)$ are the 2D plane coordinates, X coordinate, and Y coordinate of marker (b), respectively.

In the initial state t_0 when structural torsion is not presented, the direction vector $\{U_{ab}(t_0)\}^T$ of the two markers is set as the reference vector. When dynamic structural torsion occurs, the *j*-th measurement values of the two markers are used to determine the direction vector $\{U_{ab}(t_i)\}^T$ at t_i

$$\{U_{ab}(t_i)\}^T = \begin{Bmatrix} x_b(t_i) - x_a(t_i) \\ y_b(t_i) - y_a(t_i) \end{Bmatrix}^T \tag{2}$$

The direction vector size is as follows.

$$\left|\{U_{ab}(t_i)\}^T\right| = \left|\{U_{ab}(t_i)\}^T \{U_{ab}(t_i)\}\right|^{\frac{1}{2}} \tag{3}$$

A matrix that includes the initial direction vector and the *i*-th measurement direction vector can be expressed as Eq. (4).

$$\left[D(t_i)\right] = \left[\{U_{ab}(t_0)\}^T \middle| \{U_{ab}(t_i)\}^T\right] \tag{4}$$

$$=\begin{bmatrix} x_b(t_0)-x_a(t_0) & x_b(t_i)-x_a(t_i) \\ y_b(t_0)-y_a(t_0) & y_b(t_i)-y_a(t_i) \end{bmatrix}$$

$\det\left[D(t_i)\right]$ can be expressed as an equation in a form equals to a cross product of vectors. Following to cross product, those values consist of the magnitude of initial direction vector, *i*-th measurement direction vector and the angle between these two vectors.

$$\det\left[D(t_i)\right]=\left|\{U_{ab}(t_0)\}^T\{U_{ab}(t_0)\}\right|^{\frac{1}{2}}\left|\{U_{ab}(t_i)\}^T\{U_{ab}(t_i)\}\right|^{\frac{1}{2}}\sin\theta(t_i) \quad (5)$$

Therefore, the torsional angle can be represented as below, using the *i*-th 2D coordinate measurement values.

$$\theta(t_i)=\sin^{-1}\left[\frac{\det\left[D(t_i)\right]}{\left|\{U_{ab}(t_0)\}^T\{U_{ab}(t_0)\}\right|^{\frac{1}{2}}\left|\{U_{ab}(t_i)\}^T\{U_{ab}(t_i)\}\right|^{\frac{1}{2}}}\right] \quad (6)$$

In Fig. 2, based on X-axis, the sign for a clockwise torsional angle is (-) and the sign for a counterclockwise torsional angle is (+).

3.2 Torsional displacement measurement model

As structural movement occurs, displacement of a marker is accompanied by both pure rotational and translational motion. Therefore, initial coordinates of marker (a), $\{U_a(t_0)\}^T$, move to $\{U_a^R(t_i)\}^T$ at t_i because of the pure rotation, and $\{U_a^R(t_i)\}^T$ move to $\{U_a(t_i)\}^T$ because of pure translation, as shown in Fig. 3. The coordinates of structure's rotation center $\{U_c(t_i)\}^T$ are not changed by pure rotation, and the distance between the coordinates of the structure's rotation center in the initial state $\{U_c(t_0)\}^T$ and in the *i*-th measurement $\{U_c(t_i)\}^T$ represents pure translational motion of structure, denoted as TSL in Eq. (7).

$$\{TSL(t_i)\}^T=\{U_c(t_i)\}^T-\{U_c(t_0)\}^T \quad (7)$$

If the plane where Markers (a) and (b) are attached is assumed to have rigid body motion, $\{U_c(t_0)\}^T$ can be calculated from the relationship between $\{U_a(t_0)\}^T$ and $\{U_b(t_0)\}^T$. Where the plane's rotation center at t_i equals to the origin of coordination, $\{U_c(t_0)\}^T=0$ and $\{TSL(t_i)\}^T=\{U_c(t_i)\}^T$.

First, the 2D rotation conversion matrix *R* is set-up by using the *i*-th rotation angle $\theta(t_i)$, which uses the 2D coordinates of the measured markers (a) and (b).

$$\left[R(t_i)\right]=\begin{bmatrix}\cos\theta(t_i) & -\sin\theta(t_i)\\ \sin\theta(t_i) & \cos\theta(t_i)\end{bmatrix} \quad (8)$$

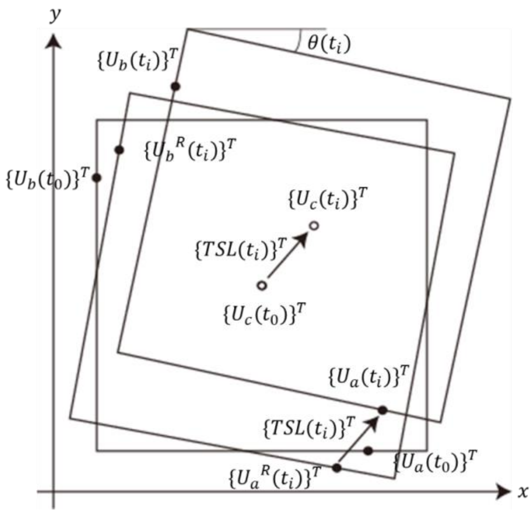

Fig. 3 Marker coordinate for torsional displacement measurement

The rotation conversion matrix rotates a specific point in the counter clockwise direction by $\theta(t_i)$ based on origin of coordination. Thus, the following relationship can be estimated.

$$\left[\{U_a^R(t_i)\}^T-\{U_c(t_0)\}^T\right]=\left[R(t_i)\right]\left[\{U_a(t_0)\}^T-\{U_c(t_0)\}^T\right] \quad (9)$$

$$\{U_a^R(t_i)\}^T=\left[R(t_i)\right]\left[\{U_a(t_0)\}^T-\{U_c(t_0)\}^T\right]+\{U_c(t_0)\}^T \quad (10)$$

$\left\{U_a^R(t_i)\right\}$ is the coordinate after the rotation conversion of marker (a) using the torsion angle at time t_i. $\left\{U_a^R(t_i)\right\}$ is a coordinate that does not consider the translational displacement occurring during structural torsion, so the translational displacement is the difference between the actual coordinates $\left\{U_a(t_i)\right\}$ of marker (a) at time t_i and the marker (a) coordinates $\left\{U_a^R(t_i)\right\}$ that only consider rotational movement.

Therefore, translational displacement can be represented by difference between $\left\{U_a(t_i)\right\}$ and $\left\{U_a^R(t_i)\right\}$, as shown in Eq. (11). Since the structure's translational displacement is constant at any point in a plane, Eq. (7) can be expressed by Eq. (12)

$$\{U_a(t_i)\}^T-\{U_a^R(t_i)\}^T=\{TSL(t_i)\}^T \quad (11)$$

$$\{TSL(t_i)\}^T=\{U_c(t_i)\}^T-\{U_c(t_0)\}^T=\{U_a(t_i)\}^T-\{U_a^R(t_i)\}^T \quad (12)$$

Finally, if substitute Eq. (10) to Eq. (12), the coordinates of the structure's center point can be obtained.

$$\{TSL(t_i)\}^T = \{U_a(t_i)\}^T - \left[R(t_i)\right]\left[\{U_a(t_0)\}^T - \{U_c(t_0)\}^T\right] - \{U_c(t_0)\}^T \quad (13)$$

The pure dynamic translational displacement of structure defined as the dynamic torsional displacement in this paper can be estimated using the torsional angle and limited number of marker coordinates.

3.3 Torsional mode identification

In Section 3.1 and 3.2, the data obtained by MCS to measure the dynamic torsional angle and displacements of x and y-axes are $\theta_k(t_i)$, $TSL_{k,x}(t_i)$, and $TSL_{k,y}(t_i)$ where $k = 1\ to\ N$, and N is the number of degrees of freedom (DOF), which are equals to the number of locations to be measured.

3.3.1 Cross power spectral density matrix

The cross power spectral density (CPSD) value in frequency domain is expressed using the torsional angle of k-th dof, $\theta_k(t_i)$, and l-th dof, $\theta_l(t_i)$.

$$R_{\theta(k)\theta(l)}(t) = \int_{-\infty}^{\infty} \theta_k(\tau)\theta_l(t+\tau)d\tau \quad (14)$$

$$S_{\theta(k)\theta(l)}(\omega) = \int_{-\infty}^{\infty} e^{-i\omega t} R_{\theta(k)\theta(l)}(t)dt \quad (15)$$

where $R_{\theta(k)\theta(l)}(t)$ is cross-correlation of $\theta_k(t)$ and $\theta_l(t)$. And, $S_{\theta(k)\theta(l)}(\omega)$ is the CPSD value for the k-th and l-th torsional angle, which is the function for the frequency domain that changes according to the angular frequency, ω.

Similarly, the CPSD for the x-axis torsional displacements is expressed using the torsional displacements for the k-th dof's x-axis $TSL_{k,x}(t_i)$ and the l-th dof's x-axis $TSL_{l,x}(t_i)$ at time t_i.

$$R_{x(k)x(l)}(t) = \int_{-\infty}^{\infty} TSL_{k,x}(\tau)TSL_{l,x}(t+\tau)d\tau \quad (16)$$

$$S_{x(k)x(l)}(\omega) = \int_{-\infty}^{\infty} e^{-i\omega t} R_{x(k)x(l)}(t)dt \quad (17)$$

where, $R_{x(k)x(l)}(t)$ and $S_{x(k)x(l)}(\omega)$ are cross-correlation and the CPSD value at the angular frequency ω for the k-th and l-th torsional displacements. Similarly, the CPSD for the y-axis torsional displacement is expressed as shown below.

$$R_{y(k)y(l)}(t) = \int_{-\infty}^{\infty} TSL_{k,y}(\tau)TSL_{l,y}(t+\tau)d\tau \quad (18)$$

$$S_{y(k)y(l)}(\omega) = \int_{-\infty}^{\infty} e^{-i\omega t} R_{y(k)y(l)}(t)dt \quad (19)$$

By combining the $S_{\theta(k)\theta(l)}(\omega)$, $S_{x(k)x(l)}(\omega)$, and $S_{y(k)y(l)}(\omega)$ values, the CPSD matrix of $S_\theta(\omega)$, $S_x(\omega)$, and $S_y(\omega)$ can be created.

$$\left[S_\theta(\omega)\right] = \begin{bmatrix} S_{\theta(1)\theta(1)}(\omega) & S_{\theta(1)\theta(2)}(\omega) & \cdots & S_{\theta(1)\theta(N)}(\omega) \\ & & & \vdots \\ & & \ddots & S_{\theta(N-1)\theta(N)}(\omega) \\ sym & & & S_{\theta(N)\theta(N)}(\omega) \end{bmatrix} \quad (20)$$

$$\left[S_x(\omega)\right] = \begin{bmatrix} S_{x(1)x(1)}(\omega) & S_{x(1)x(2)}(\omega) & \cdots & S_{x(1)x(N)}(\omega) \\ & & & \vdots \\ & & \ddots & S_{x(N-1)x(N)}(\omega) \\ sym & & & S_{x(N)x(N)}(\omega) \end{bmatrix} \quad (21)$$

$$\left[S_y(\omega)\right] = \begin{bmatrix} S_{y(1)y(1)}(\omega) & S_{y(1)y(2)}(\omega) & \cdots & S_{y(1)y(N)}(\omega) \\ & & & \vdots \\ & & \ddots & S_{y(N-1)y(N)}(\omega) \\ sym & & & S_{y(N)y(N)}(\omega) \end{bmatrix} \quad (22)$$

3.3.2 Singular value decomposition

Singular value decomposition (SVD) is used to decompose CPSD matrices. In linear algebra, SVD is a factorization of a real complex matrix.

$$\left[S_\theta(\omega)\right] = \left[U_\theta(\omega)\right] \times \left[\mathrm{SV}_\theta(\omega)\right] \times \left[\mathrm{V}_\theta(\omega)\right] \quad (23)$$

$$\left[S_x(\omega)\right] = \left[U_x(\omega)\right] \times \left[\mathrm{SV}_x(\omega)\right] \times \left[\mathrm{V}_x(\omega)\right] \quad (24)$$

$$\left[S_y(\omega)\right] = \left[U_y(\omega)\right] \times \left[\mathrm{SV}_y(\omega)\right] \times \left[\mathrm{V}_y(\omega)\right] \quad (25)$$

where $\left[\mathrm{SV}_\theta(\omega)\right]$, $\left[\mathrm{SV}_x(\omega)\right]$, and $\left[\mathrm{SV}_y(\omega)\right]$ are all rectangular diagonal matrices, and U, V are complex unitary matrices holding the singular vectors.

$$\left[SV_\theta(\omega)\right] = \begin{bmatrix} SV_{\theta 11}(\omega) & 0 & \cdots & 0 \\ & SV_{\theta 22}(\omega) & & \vdots \\ & & \ddots & 0 \\ sym & & & SV_{\theta NN}(\omega) \end{bmatrix} \quad (26)$$

$$\left[SV_x(\omega)\right] = \begin{bmatrix} SV_{x11}(\omega) & 0 & \cdots & 0 \\ & SV_{x22}(\omega) & & \vdots \\ & & \ddots & 0 \\ sym & & & SV_{xNN}(\omega) \end{bmatrix} \quad (27)$$

$$\left[SV_y(\omega)\right] = \begin{bmatrix} SV_{y11}(\omega) & 0 & \cdots & 0 \\ & SV_{y22}(\omega) & & \vdots \\ & & \ddots & 0 \\ sym & & & SV_{yNN}(\omega) \end{bmatrix} \quad (28)$$

3.3.3 Natural frequency

$\left[\mathrm{SV}_\theta(\omega)\right]$, $\left[\mathrm{SV}_x(\omega)\right]$, and $\left[\mathrm{SV}_y(\omega)\right]$ can be used to draw a singular value curve. In general, the first value among several singular values in $\mathrm{SV}(\omega)$ is used. Further details on the SVD are provided by Brincker *et al*. (2001). In a singular value curve, the horizontal axis is frequency and the vertical axis is the singular values. The torsional angle and displacements are used to draw three curves: $\mathrm{SV}_{\theta 11}(\omega)$, $\mathrm{SV}_{x11}(\omega)$, and $\mathrm{SV}_{y11}(\omega)$. When this curve draw the peak, the frequency that corresponds to the peak can be considered as the structure's natural frequency. The structure's *k*-th natural frequency is called ω_k where $k=1\ to\ M$, and M is the number of modes. Because the number of modes that can be identified is usually the same as the number of DOF, $M=N$.

3.3.4 Mode shape

Below is a matrix of $\left[U_\theta(\omega_k)\right]$ derived from SVD at *k*-th natural frequency, ω_k.

$$\left[U_\theta(\omega_k)\right]=\begin{bmatrix} U_{\theta 11}(\omega_k) & U_{\theta 12}(\omega_k) & \cdots & U_{\theta 1N}(\omega_k) \\ U_{\theta 21}(\omega_k) & U_{\theta 11}(\omega_k) & & \vdots \\ \vdots & & \ddots & U_{\theta(N-1)N}(\omega_k) \\ U_{\theta N1}(\omega_k) & \cdots & U_{\theta N(N-1)}(\omega_k) & U_{\theta NN}(\omega_k) \end{bmatrix} \tag{29}$$

where $\left\{U_\theta^{mode}(\omega_k)\right\}$ from the first column of $\left[U_\theta(\omega_k)\right]$ are complex numbers, and the imaginary parts of these values are the structure's *k*-th unnormalized torsional mode shape. Similarly, the structure's *k*-th unnormalized translational mode shape can be obtained from the first column of $\left[U_x(\omega_k)\right]$ and $\left[U_y(\omega_k)\right]$.

$$\left\{U_\theta^{mode}(\omega_k)\right\}=\begin{Bmatrix} U_{\theta 11}(\omega_k) \\ U_{\theta 21}(\omega_k) \\ \vdots \\ U_{\theta N1}(\omega_k) \end{Bmatrix}$$

$$\left\{U_x^{mode}(\omega_k)\right\}=\begin{Bmatrix} U_{x11}(\omega_k) \\ U_{x21}(\omega_k) \\ \vdots \\ U_{xN1}(\omega_k) \end{Bmatrix} \tag{30}$$

$$\left\{U_y^{mode}(\omega_k)\right\}=\begin{Bmatrix} U_{y11}(\omega_k) \\ U_{y21}(\omega_k) \\ \vdots \\ U_{yN1}(\omega_k) \end{Bmatrix}$$

$\left\{\phi_\theta^C(\omega_k)\right\}$, $\left\{\phi_x^C(\omega_k)\right\}$, and $\left\{\phi_y^C(\omega_k)\right\}$ are the torsional, X-axis translational, and Y-axis translational mode shapes, respectively.

$$\left\{\phi_\theta^C(\omega_k)\right\}=\begin{Bmatrix} imag(U_{\theta 11}(\omega_k)) \\ imag(U_{\theta 21}(\omega_k)) \\ \vdots \\ imag(U_{\theta N1}(\omega_k)) \end{Bmatrix}$$

$$\left\{\phi_x^C(\omega_k)\right\}=\begin{Bmatrix} imag(U_{x11}(\omega_k)) \\ imag(U_{x21}(\omega_k)) \\ \vdots \\ imag(U_{xN1}(\omega_k)) \end{Bmatrix} \tag{29}$$

$$\left\{\phi_y^C(\omega_k)\right\}=\begin{Bmatrix} imag(U_{y11}(\omega_k)) \\ imag(U_{y21}(\omega_k)) \\ \vdots \\ imag(U_{yN1}(\omega_k)) \end{Bmatrix}$$

3.3.5 Three-dimensional mode shape

The structure's *k*-th 3D mode shape is a combination of $\left\{\phi_\theta^C(\omega_k)\right\}$, $\left\{\phi_x^C(\omega_k)\right\}$, and $\left\{\phi_y^C(\omega_k)\right\}$. The ratio by which each of $\left\{\phi_\theta^C(\omega_k)\right\}$, $\left\{\phi_x^C(\omega_k)\right\}$, and $\left\{\phi_y^C(\omega_k)\right\}$ contributes to the structure's *k*-th 3D mode shape is the same as the ratio of $SV_{11}(\omega_k)$ in the first row and first column of $\left[SV(\omega_k)\right]$ found in Section 3.3.2 where $k=1\ to\ M$, M is the number of modes.

$$\left\{\phi_\theta(\omega_k)\right\}=SV_{\theta 11}(\omega_k)\times\{\phi_\theta^C(\omega_k)\} \tag{32}$$

$$\left\{\phi_x(\omega_k)\right\}=SV_{x11}(\omega_k)\times\{\phi_x^C(\omega_k)\} \tag{33}$$

$$\left\{\phi_y(\omega_k)\right\}=SV_{y11}(\omega_k)\times\{\phi_y^C(\omega_k)\} \tag{34}$$

4. Application

4.1 Experimental setup

To verify the torsion measurement model presented in this research, vibration tests for a three-story shear frame specimen was performed. The target structure’s geometric dimensions can be seen in Fig. 4(a). The specimen has symmetric plan with 305 mm in both the x and y directions. All columns have the same square bar section of 6 x 6 mm. The elastic modulus and yield strength of the steel in the specimen are 206 GPa and 235.3 MPa, respectively. Four markers were attached to each floor, so a total of 12 markers (M1–M12) were used. And, three VICON T-160 MCS cameras were installed around the structure to capture the movement of the markers (Vicon Motion Systems Ltd). The movement of the attached markers (M1–M12) in three dimensions and the widely used LDSs (L1–L4) were used to measure and compare the structure's torsional responses. The sensor installation locations are shown in Fig. 4(b). To induce torsion to the specimen, the corner (D) of the

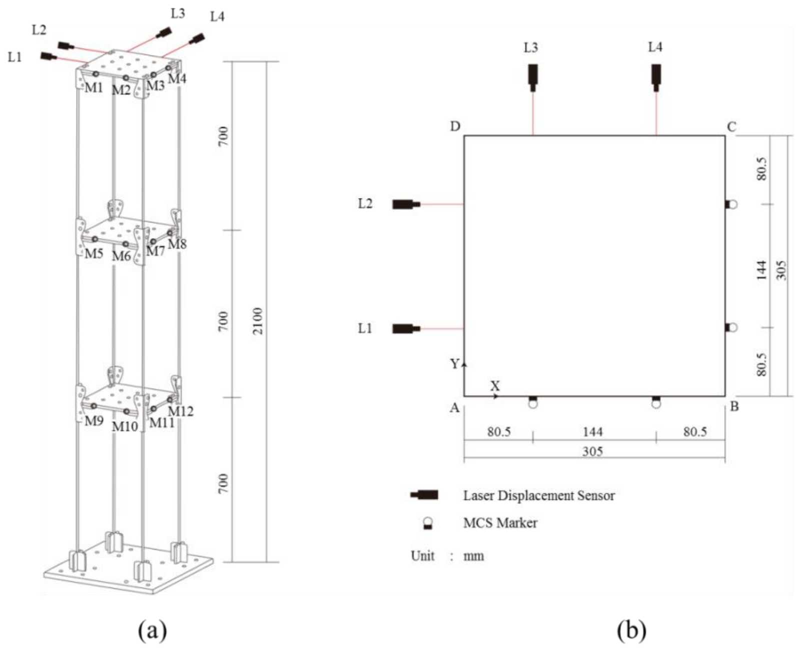

Fig. 4 Experimental setup: (a) target structure and (b) sensor layout

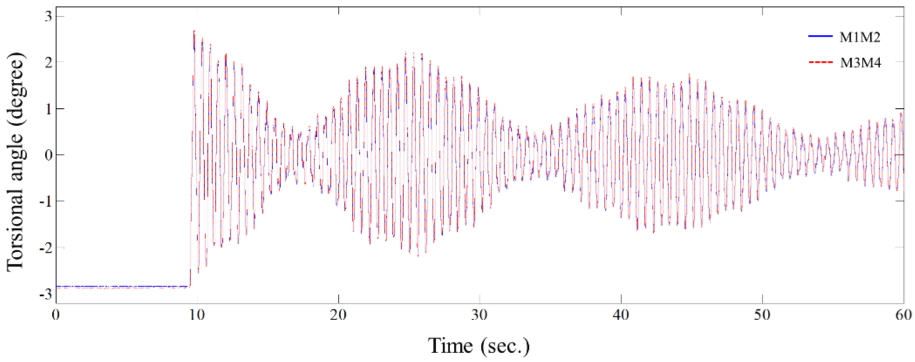

Fig. 5 Dynamic torsional angle measured from MCS

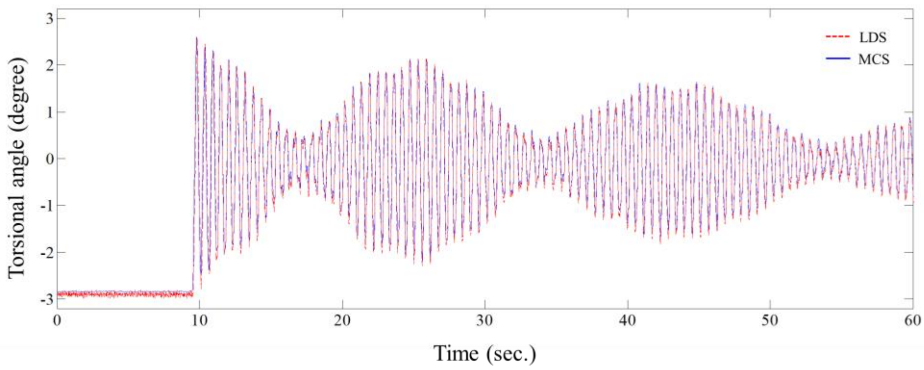

Fig. 6 Comparison of dynamic torsional angles between MCS and LDS

Table 1 Comparison of dynamic torsional angles for six cases (M1M2-M3M4)

Time (sec.)	M1M2 (°)	M1M3 (°)	M1M4 (°)	M2M3 (°)	M2M4 (°)	M3M4 (°)	Maximum differences (°)
9.84	2.587	2.667	2.694	2.731	2.668	2.685	0.144
24.80	2.134	2.214	2.202	2.282	2.234	2.239	0.148
44.88	1.655	1.694	1.710	1.725	1.731	1.750	0.095
64.97	1.269	1.297	1.288	1.320	1.303	1.316	0.051
92.41	0.932	0.957	0.976	0.979	0.989	0.996	0.064
122.08	0.614	0.615	0.62	0.615	0.6274	0.643	0.029

Table 2 Comparison of torsional angles at six time steps between MCS and LDS

	LDS	MCS	Relative error (%)	Absolute error (°)
Time (s)	Angle (°)	Angle (°)		
9.85	2.593	2.587	-0.23	-0.006
24.74	2.120	2.134	0.66	0.014
44.81	1.593	1.655	3.75	0.062
64.91	1.253	1.269	1.26	0.016
92.37	0.869	0.932	6.76	0.063
121.88	0.585	0.614	4.72	0.029

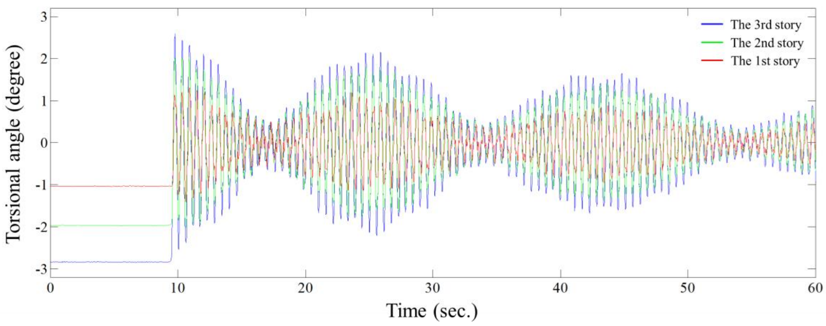

Fig. 7 Global responses of dynamic torsional angles from MCS

structure's top floor was pulled obliquely. Through the test pulling with the diagonal-direction initial displacement and releasing the specimen, the free vibrations were generated. The structure's responses were measured for about 1 min (60 s), and Eqs. (6) and (13) were used to calculate the torsional angle and displacement.

4.2 Measurement of torsional responses

4.2.1 Measurement of torsional angle

The results of torsional angle that occurs on the top floor of the target structure measured using MCS are shown in Fig. 5. As explained in Section 3.1, at least two markers are needed to measure the torsional angle using MCS. The number of cases where two of the M1–M4 markers installed on the top floor are selected is six (M1M2-M3M4), as listed in Table 1. The results of the structure's torsional angle when using M1 and M2 with the label M1M2 and using M3 and M4 with the label M3M4 are shown in Fig. 5. Table 1 compares the torsional angles in more detail for each of the six cases (M1M2-M3M4) at some time steps when a large amount of torsional angle occurs. Depending on which markers were selected for calculating the torsional angle, the differences of torsional angle were a minimum of 0.029° and a maximum of 0.148°.

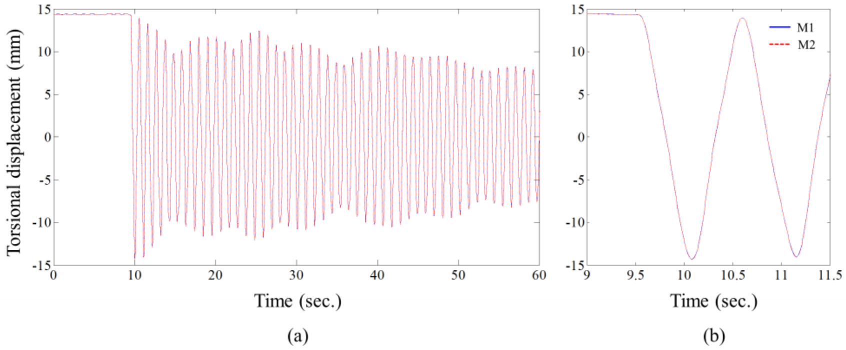

Fig. 8 X-direction of dynamic torsional displacement from MCS: (a) 0~60 seconds, (b) 9~11.5seconds

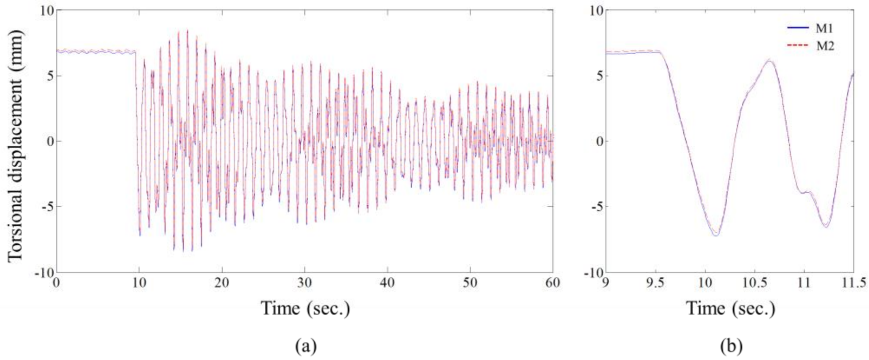

Fig. 9 Y-direction of dynamic torsional displacement from MCS: (a) 0~60 seconds, (b) 9~11.5seconds

The torsional angles measured by MCS and LDS are compared in Fig. 6. The method to calculate the torsional angle using displacements obtained from LDS is provided in Appendix B. The blue line is the torsional angle obtained using M1 and M2, and the red line is the torsional angle obtained using LDS L3 and L4. Table 2 gives a comparison of the torsional angles obtained using LDS and MCS at some time steps when a large amount of torsional behaviors occurs. The relative error is calculated as $\theta_{MCS} - \theta_{LDS} / \theta_{MCS}$, and the absolute error is calculated as $\theta_{MCS} - \theta_{LDS}$. At a time step of 9.85 s, when the torsional angle was largest, the absolute error was at its smallest at 0.006°, and the relative error was at its smallest at -0.23%. At 92.37 s, the largest absolute error of 0.063° was observed and the relative error was 6.76%.

MCS can be used to measure the overall torsional responses of the target structure by simple installation of the markers. Eq. (6) can be applied to each floor to measure the torsional angle of the three-story shear frame, and the results are shown in Fig. 7. When the structure's initial displacement occurs, the torsional angles were -1.03° on the 1st floor, -1.96° on the 2nd floor, and -2.84° on the 3rd floor.

4.2.2 Measurement of torsional displacement

Eq. (13) can be used to calculate the inherent translational displacement in torsion. And, results from this calculation are called as torsional displacement in this paper. The torsional angle measured in Section 4.2.1 and the displacements measured at a marker can be used to calculate the x- and y-directional torsional displacement according to the x-y coordinates shown in Fig. 4(b). The number of cases where one of the measurement points is selected is four (M1~M4). From these cases, displacements from M1 and M2 were used to calculate dynamic torsional displacements and the results were compared in Figs. 8 and 9.

Figs. 8(a) and 9(a) show a comparison of the x- and y-axes torsional displacements for the period of 0~60 seconds. Figs. 8(b) and 9(b) are the magnification of Figs. 8(a) and 9(a) for the period of 9~11.5 seconds. The blue line is the torsional displacement measured from the displacement of M1 and the torsional angle obtained from M1M2. The red line is the torsional displacement measured from the displacement of M2 and the torsional angle obtained from M1M2. According to Fig. 8(a), before the vibration started, the x-directional torsional displacement using M1 was 14.43 mm, and the torsional displacement using M2 was 14.42 mm, showing an error of 0.01 mm. This is less than the MCS measurement limit of 0.06 mm (Park *et al.* 2015b), confirming that the x-directional torsional displacement was accurately measured. Similarly, according to Fig. 9(a), the y-directional torsional displacement using M1 was 6.76 mm, and using M2 it was 6.77 mm, showing an error of 0.01 mm and confirming that the y-direction was also measured accurately.

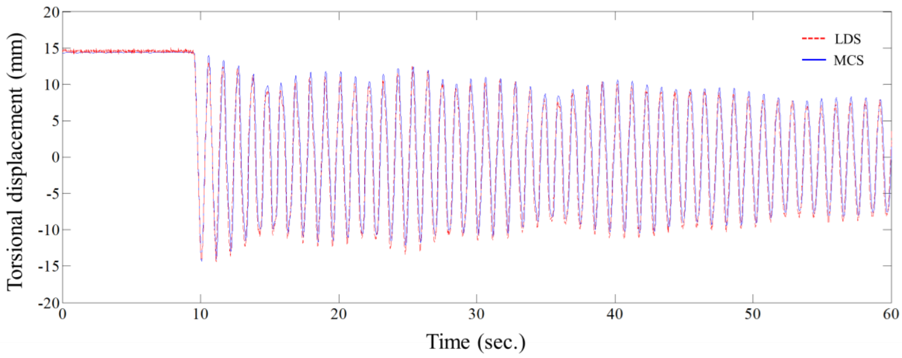

Fig. 10 Comparison of x-direction of dynamic torsional displacement between MCS and LDS

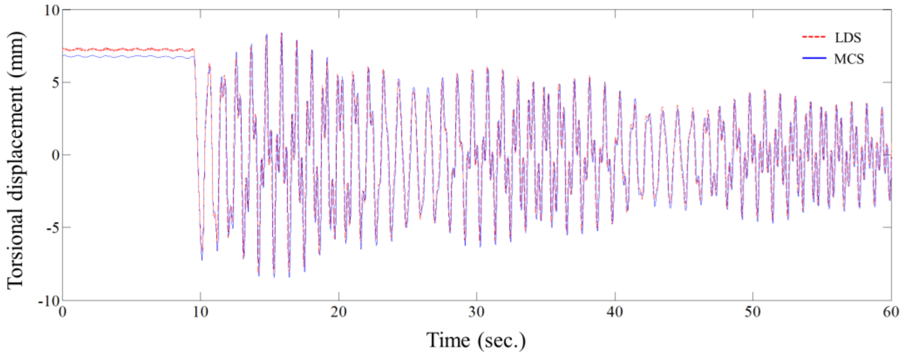

Fig. 11 Comparison of y-direction of dynamic torsional displacement between MCS and LDS

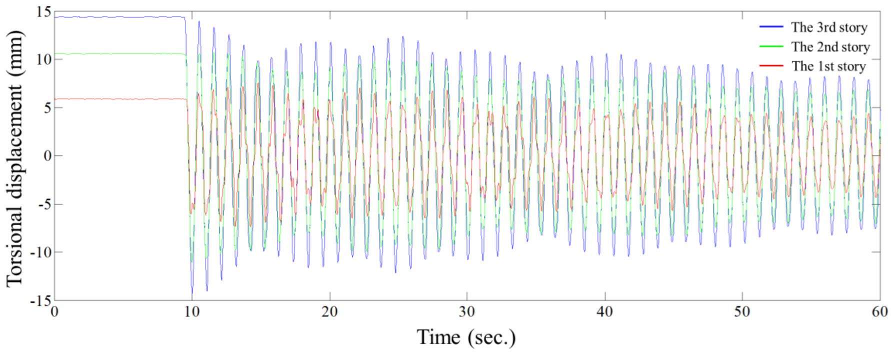

Fig. 12 Global responses of x-directional dynamic torsional displacements from MCS

Table 3 Comparison of torsional displacement between MCS and LDS

	LDS (mm)	MCS (mm)	Relative error (%)	Absolute error (mm)
x-direction	14.64	14.43	-1.45	-0.21
y-direction	7.27	6.76	-7.54	-0.51

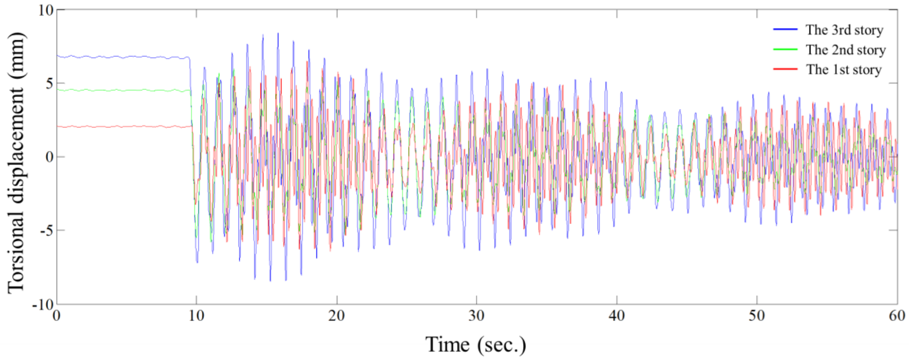

Fig. 13 Global responses of y-directional dynamic torsional displacements from MCS

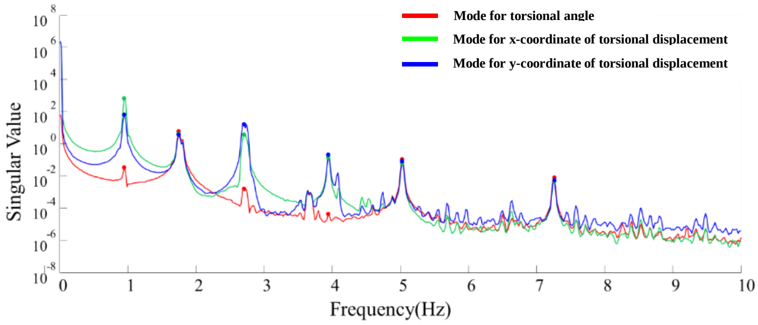

Fig. 14 Singular value curves from MCS-measured dynamic torsional responses

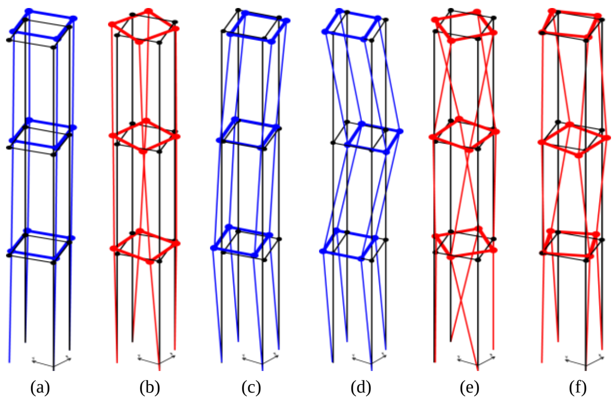

Fig. 15 Mode shapes from MCS-measured dynamic torsional responses

Figs. 10 and 11 show comparisons of the torsional displacements in the structure's top floor using LDS and MCS. The blue and red lines are the torsional displacements extracted from measurements of MCS and LDS, respectively. For MCS, the displacement of M1 and the torsional angle calculated from M1M2 were used. Table 3 shows the average displacement at 0~9 seconds, before vibration occurred.

From the error analysis of LDS as provided in Appendix C, there are some limitations for installing LDS sensors.

The distance between LDSs must be known exactly and the LDSs must be installed perpendicular to the measurement target surface. Under the measuring conditions with satisfying the constraints for sensor installation, LDS can make relatively accurate measurements. However, actually satisfying the limiting conditions is difficult, in practical. During the tests using LDS, measurement errors were generated due to the strict sensor installation conditions. Thus, as shown in Table 3, some errors between MCS and LDS occurred at initial time steps before vibrating.

Table 4 Results of system identification

	Frequency (Hz)	Modes
1st mode	0.94	For torsional displacements
2nd mode	1.74	For torsional angle
3rd mode	2.70	For torsional displacements
4th mode	3.96	For torsional displacements
5th mode	5.02	For torsional angle
6th mode	7.26	For torsional angle

Eq. (13) was applied to each floor of the test structure, and the structure's overall torsional displacement responses were measured. The x- and y-directional dynamic torsional displacement responses for each floor of the target structure are shown in Figs. 12-13, respectively.

4.3 Measurement of torsional modal parameters

Using the MCS torsion measurements, estimation of modal parameters such as natural frequency and mode shape was performed for the target structure. The dynamic displacement measured from the markers attached to the target test structure was applied to the model presented in Section 3.3, and the dynamic torsional angle of each floor and the dynamic torsional displacement of the center were calculated. The dynamic torsion angle and displacement calculated in Section 4.2 were used to perform frequency domain decomposition (Brincker 2000), which is a method for obtaining the dynamic properties of frequency domains, and the natural frequency and mode shape were obtained. The center of each floor's x- and y-axes dynamic torsional displacement, and dynamic torsional angle obtained from Eqs. (6) and (13) were each used to create three CPSD functions. For this, the number of data segments in frequency domain (NFFT) was 5000, the window was of Hanning type, and the averaging rate was 50%. Fig. 14 shows the singular values obtained from SVD on each CPSD function.

The frequency which corresponds to the peak of singular value can be considered as the natural frequency of the target structure. The natural frequencies of the target structure were 0.94, 1.74, 2.70, 3.96, 5.02, and 7.26 (Hz). From the Fig. 14, it can be supposed that the natural frequencies for the peaks in the curve obtained from the torsional angle are 1.74, 5.02, and 7.26 (Hz). The remaining peaks of 0.94, 2.70, and 3.96 (Hz) where large amplitudes of singular values from torsional displacements occur are expected to be modes for torsional displacements. The mode shapes were obtained for the first six modes at natural frequencies mentioned above, as shown in Fig. 15.

Based on results of the extracting of the mode shapes for all modes, it was confirmed that the 1st, 3rd, and 4th mode shape results were modes for torsional displacements, and the 2nd, 5th, and 6th were modes for torsional angle. Table 4 lists the results of system identification for the target structure using MCS.

In the test, the structure's initial displacement was oblique, but closer to the x-direction than the y-direction. Thus, because of effect of initial condition in the test, the mode shape for the 1st mode, which was the main deformation mode, the x-coordinate in torsional displacements was predominant. However, for the 3rd and 4th mode which have lower influences on the responses of structure, mode shapes that combined the x- and y-coordinate of torsional displacements occurred. In the 2nd, 5th, and 6th modes, the mode shapes for torsional angle were clearly represented by the proposed model. Thus, it is confirmed that MCS can be used to identify the torsional modal properties as well as to measure the torsional rotation and displacements of the structures.

5. Conclusions

This paper presented a dynamic torsional response measurement model that can measure the torsional angle and displacement using an MCS, which is a non-contact vision-based monitoring system that measures dynamic displacement by tracking markers attached to the structure. In addition, the model provides the identification method for the torsional modal parameters, natural frequency and mode shape. To verify the proposed model, vibration tests were performed using a three-story shear frame specimen. Applying the dynamic displacements measured by the MCS to the presented model, the dynamic torsional responses were obtained.

In the study, six cases (M1M2~M3M4) of different MCS markers (measurement points) were considered to obtain the torsional angles. When all the cases were compared, it was confirmed that the torsional angle was stably measured with an absolute difference below a maximum of 0.15°. Moreover, through comparison of the torsional angles obtained using MCS versus those obtained using LDS, it was confirmed that the torsional angle was measured with a relative difference below 6.76%. The torsional displacements obtained from the presented model for all cases show 0.01 mm difference for both X and Y directions, which is below the MCS measurement accuracy limit of 0.06 mm. Moreover, when the torsional displacements from LDS measurements were compared to those of MCS, a relative difference within 7.54% was generated; the difference was considered to be induced from the non-perfect installation condition of the LDS. The measured dynamic torsional responses, which include the structure's torsional angle and displacements, were used to extract the modal parameters. The structure's modes for torsional angle and displacement were clearly identified via the presented model. However, there are some limitations of the current MCS technology for application in SHM of real-life structures. Since the measurement range of MCS is less than approximately 50 m, the presented model using MCS is limited to apply to the torsional monitoring for large-scale structures. In the majority of cases, several cameras for tracking markers in a target structure are installed at the ground around the target structure. Thus, the vibrations around the ground where cameras are installed should be controlled. If the ground around cameras is not isolated to the target structure, MCS is limited to measure the torsional movement of the target structure subject to ground motion such as earthquake.

Acknowledgments

This work was supported by the National Research Foundation of Korea (NRF) grand funded by the Korea government (Ministry of Science, ICT & Future Planning, MSIP) (No. 2016R1A6A3A11932881).

References

Ansari, F. (1997), "State-of-the-art in the applications of fiber-optic sensors to cementitious composites", *Cement Concrete Comp.*, **19**(1), 3-19.

Breuer, P., Chmielewski, T., Orski, P.G. and Konopka, E. (2002), "Application of GPS technology to measurements of displacements of high-rise structures due to weak winds", *J. Wind Eng. Ind. Aerod.*, **90**(3), 223-230.

Brincker, R., Zhang, L. and Andersen, P. (2001), "Modal identification of output-only systems using frequency domain decomposition", *Smart Mater. Struct.*, **10**(3), 441-445.

Casciati, F. and Fuggini, C. (2011), "Monitoring a steel building using GPS sensors", *Smart Struct. Syst.*, **7**(5), 349-363.

Celebi, M. and Sanli, A. (2002), "GPS in pioneering dynamic monitoring of long-period structures", *Earthq. Spectra*, **18**(1), 47-61.

Chan, W.S., Xu, Y.L., Ding, X.L., Xiong, Y.L. and Dai, W.J. (2006), "Assessment of dynamic measurement accuracy of GPS in three directions", *J. Surv. Eng.-ASCE*, **132**(3), 108-117.

Chen, L., Zhang, W.G., Wang, L., Zhang, H., Sieg, J., Zhou, Q., Zhang, L.Y., Wang, B. and Yan, T.Y. (2014), "In-fiber torsion sensor based on dual polarized Mach-Zehnder interference", *Opt. Express*, **22**(26), 31654-31664.

Chen, W., Lou, S., Wang, L., Zou, H., Lu, W. and Jean, S. (2011), "Highly sensitive torsion sensor based on sagnac interferometer using side-leakage photonic crystal fiber", *IEEE Photonic. Tech. L.*, **23**(21), 1639-1641.

Choi, S.W., Kim, I.S., Park, J.H., Kim, Y., Sohn, H.G. and Park, H.S. (2013), "Evaluation of stiffness changes in a high-rise building by measurements of lateral displacements using GPS technology", *Sensors*, **13**(11), 15489-15503.

Duffey, T.A., Doebling, S.W., Farrar, C.R., Baker, W.E. and Rhee, W.H. (2001), "Vibration-based damage identification in structures exhibiting axial torsional responses", *J. Vib. Acoust.*, **123**(1), 84-91.

Frangopol, D.M., Strauss, A. and Kim, S. (2008), "Use of monitoring extreme data for the performance prediction of structures: General approach", *Eng. Struct.*, **30**(12), 3644-3653.

Fraser, C.S. and Riedel, B. (2000), "Monitoring the thermal deformation of steel beams via vision metrology", *ISPRS-J. Photogramm. Remote Sens.*, **55**(4), 268-276.

Im, S.B., Cloudt, G.C., Fogle, J.A. and Hurlebaus, S. (2013), "Enhanced damage index method using torsion modes of structures", *Smart Struct. Syst.*, **12**(3-4), 427-440.

Jang, S., Jo, H., Cho, S., Mechitov, K., Rice, J.A., Sim, S.H., Jung, H.J., Yun, C.B., Spencer Jr., B.F. and Agha, G. (2010), "Structural health monitoring of a cable-stayed bridge using smart sensor technology: Development and evaluation", *Smart Struct. Syst.*, **6**(5-6), 439-459.

Jeon, H., Kim, Y., Lee, D. and Myung, H. (2014), "Vision-based remote 6-DOF structural displacement monitoring system using a unique marker", *Smart Struct. Syst.*, **13**(6), 927-942.

Juang, J.C. (2000), "On GPS positioning and integrity monitoring", *IEEE T. Aero. Elec. Sys.*, **36**(1), 327-336.

Keyence Co. (2016), *IL Series Instruction Manual*, http://www.keyence.com

Lava, P., Cooreman, S. and Debruyne, D. (2010), "Study of systematic errors in strain fields obtained via DIC using heterogeneous deformation generated by plastic FEA", *Opt. Lasers Eng.*, **48**(4), 457-468.

Lovse, J., Teskey, W., Lachapelle, G. and Cannon, M. (1995), "Dynamic deformation monitoring of tall structure using GPS technology," *J. Surv. Eng.-ASCE*, **121**(1), 35-40.

Ni, Y.Q., Xia, Y., Lin, W., Chen, W.H. and Ko, J.M. (2012), "SHM benchmark for high-rise structures: A reduced-order finite element model and field measurement data", *Smart Struct. Syst.*, **10**(4), 411-426.

Oh, B.K., Hwang, J.W., Kim, Y., Cho, T. and Park, H.S. (2015), "Vision-based system identification technique for building structures using a motion capture system", *J. Sound Vib.*, 356, 72-85.

Olaszek, P. (1999), "Investigation of the dynamic characteristic of bridge structures using a computer vision method", *Measurement*, **25**(3), 227-236.

NaturalPoint, Inc. DBA OptiTrack. (2016), http://www.optitrack.com/

Park, H.S., Sohn, H.G., Kim, I.S. and Park, J.H. (2008), "Application of GPS to monitoring of wind-induced responses of high-rise buildings", *Struct. Des. Tall Spec. Build.*, **17**(1), 117-132.

Park, H.S., Park, K.H., Kim, Y. and Choi, S.W. (2015a), "Deformation monitoring of a building structure using a motion capture system", *IEEE/ASME T. Mech.*, **20**(5), 2276-2284.

Park, J.W., Sim, S.H. and Jung, H.J. (2013), "Displacement estimation using multimetric data fusion", *IEEE/ASME Trans. Mechatronics*, **18**(6), 1675-1682.

Park, S.W., Park, H.S., Kim, J. and Adeli, H. (2015b), "3D displacement measurement model for health monitoring of structures using a motion capture system", *Measurement*, **59**, 352-362.

Roberts, G.W., Dodson, A.H. and Ashkenazi, V. (1999), "Twist and deflect: monitoring motion of the Humber Bridge", *GPS World*, **10**(10), 24-34.

Roberts, G.W., Meng, X. and Dodson, A.H. (2004), "Integrating a global positioning system and accelerometers to monitor the deflection of bridges", *J. Surv. Eng.-ASCE*, **130**(2), 65-72.

Vicon Motion Systems Ltd. (2016), http://www.vicon.com/

Yacamini, R., Smith, K.S. and Ran, L. (1998), "Monitoring torsional vibrations of electro-mechanical systems using stator currents", *J. Vib. Acoust.*, **120**(1), 72-79.

Yang, R., Bao, H., Zhang, S., Ni, K., Zheng, Y. and Dong, X. (2015), "Simultaneous measurement of tilt angle and temperature with pendulum-based fiber bragg grating sensor", *IEEE Sens. J.*, **15**(11), 6381-6384.

Yi, T.H., Li, H.N. and Gu, M. (2013), “Wavelet based multi-step filtering method for bridge health monitoring using GPS and accelerometer”, *Smart Struct. Syst*., **11**(4), 331-348.

Yoshida, S., Dyke, S.J., Giacosa, L.M. and Truman, K.Z. (2003), “Experimental verification of torsional response control of asymmetric buildings using MR dampers”, *Earthq. Eng. Struct. D.*, **32**(13), 2085-2105.

Zhang, W., Kai, G., Dong, X., Yuan, S. and Zhao, Q. (2002), “Temperature-independent FBG-type torsion sensor based on combinatorial torsion beam”, IEEE *Photonic. Tech. L*., **14**(8), 1154-1156.

HJ

Appendix

A. Euler coordinate transform

After the marker and camera setup is complete in MCS measurement, a T-shape wand coordinate system is created and the movement of markers within this coordinate system is measured. Euler 3D rotation conversion is used to convert the T-shape wand coordinate system to a structural coordinate system. The matrix $\left[R_s\right]$ which converts the wand coordinate system to a structural coordinate system is shown in Eq. (A1).

$$\begin{Bmatrix} X \\ Y \\ Z \end{Bmatrix} = \left[R_s\right] \begin{Bmatrix} x \\ y \\ z \end{Bmatrix} = \begin{bmatrix} 1 & 0 & 0 \\ 0 & \cos\theta_x & -\sin\theta_x \\ 0 & \sin\theta_x & \cos\theta_x \end{bmatrix} \begin{bmatrix} \cos\theta_y & 0 & -\sin\theta_y \\ 0 & 1 & 0 \\ \sin\theta_y & 0 & \cos\theta_y \end{bmatrix} \begin{bmatrix} \cos\theta_z & -\sin\theta_z & 0 \\ \sin\theta_z & \cos\theta_z & 0 \\ 0 & 0 & 1 \end{bmatrix} \begin{Bmatrix} x \\ y \\ z \end{Bmatrix} \quad \text{(A1)}$$

The angles θ_x , θ_y , and θ_z can be extracted from the vector operation. In more details refer to Park *et al*. (2015b).

B. Measurement of torsional angle using LDS

In this study, to compare the torsional response measured by MCS with an existing displacement measurement sensor, LDS was used. The sensors are installed opposite to the measurement point of target structure, and the distance between the sensor and the measurement point is measured in order to measure the structure's movement.

An installation like the one shown in Fig. B1 is required to measure the structure's planar movement when structural torsion occur, disregarding deformation in the direction of gravity. Before occurrence of movement, LDS L1 and L3 are installed at x_T and y_T distance from the corner $A(0,0)$ of the structure along the x- and y-direction, and LDS L2 and L4 are installed l distance from the LDS installed for each axis. If corner of plate is right-angle and structure has rigid diaphragm of infinite stiffness in planar, torsional angles of each side are same. Therefore, at least two LDS measurement from same side can be used to calculate the torsional angle using Eqs. (B1) and (B2).

$$\theta = \cos^{-1}\left(\frac{\overrightarrow{AB}\cdot\overrightarrow{A_iB_i}}{\left|\overrightarrow{AB}\right|\left|\overrightarrow{A_iB_i}\right|}\right) = \cos^{-1}\left(\frac{l}{\sqrt{l^2+(L_{2i}-L_{1i})^2}}\right) \quad \text{(B1)}$$

$$\text{for} \quad L_{2i}-L_{1i} > 0$$

$$\theta = -\cos^{-1}\left(\frac{\overrightarrow{AB}\cdot\overrightarrow{A_iB_i}}{\left|\overrightarrow{AB}\right|\left|\overrightarrow{A_iB_i}\right|}\right) = -\cos^{-1}\left(\frac{l}{\sqrt{l^2+(L_{2i}-L_{1i})^2}}\right) \quad \text{(B1)}$$

$$\text{for}\, L_{2i}-L_{1i} < 0$$

Eqs. (B1) and (B2) use the inner product of $\overrightarrow{AB}$ and $\overrightarrow{A_iB_i}$. $\overrightarrow{A_iB_i}$ is direction vector at time t_i when torsion is occurring. If $i=0$, $\overrightarrow{A_iB_i}$ is same as $\overrightarrow{AB}$ in initial state of structure. L_{1i} and L_{2i} are the LDS1 and LDS2 measurement data at time t_i . The intersection point $A(a,b)$ in Fig. B1 can be described in Eqs. (B3) and (B4).

$$a = \frac{\left(L_{2i}-L_{1i}\right)\left(L_{4i}-L_{3i}\right)x_T + l\left(x_T-L_{1i}\right)\left(L_{4i}-L_{3i}\right) - l^2L_{3i}}{\left(L_{2i}-L_{1i}\right)\left(L_{4i}-L_{3i}\right)-l^2} \quad \text{(B3)}$$

$$b = \frac{\left(L_{2i}-L_{1i}\right)\left\{\left(L_{2i}-L_{1i}\right)\left(L_{4i}-L_{3i}\right)x_T + l\left(x_T-L_{1i}\right)\left(L_{4i}-L_{3i}\right) - l^2L_{3i}\right\}}{l\left(L_{2i}-L_{1i}\right)\left(L_{4i}-L_{3i}\right)-l^3} - \frac{x_T\left(L_{2i}-L_{1i}\right)}{l} + L_{1i} \quad \text{(B4)}$$

The Eqs. (B3) and (B4) can be solved through a system of equation using measurement data of LDS1 and LDS2 and a using measurement data of LDS3 and LDS4. Besides the pure rotation, to calculate the structure's torsional displacement along with the x- and y-axes, coordinate for each structure's corners is needed. The coordinates for each corner can be calculated through the length of each of the structure's sides and the coordinates of intersection point A calculated by Eq. (B3), as shown in Fig. B1. The corner coordinates can be used to finally calculate the structure's center coordinates.

C. Error analysis of measurement using LDS

The measurement data from the two installed LDSs can be used to calculate the torsional angle through Eqs. (B1) and (B2). However, there are two assumptions when installing the LDS to calculate torsional displacement precisely: (a) the distance between LDSs is known and (b) the LDS is installed at a right angle to the structure.

To measure accurately the distance between LDSs is fairly difficult. Therefore, errors can occur due to the in-exactly measured distance between LDSs, as shown in Fig. C1. The distance between two LDSs is assumed to be $l\,mm$, but when an error of the distance has a value of $\pm\Delta l\ mm$, a measurement value of LDS occurs an error of $\Delta l\tan\theta$ according to the structure's torsional angle θ . Because of this measurement error, the torsional angle equation is modified as in Eqs. (C1) and (C2).

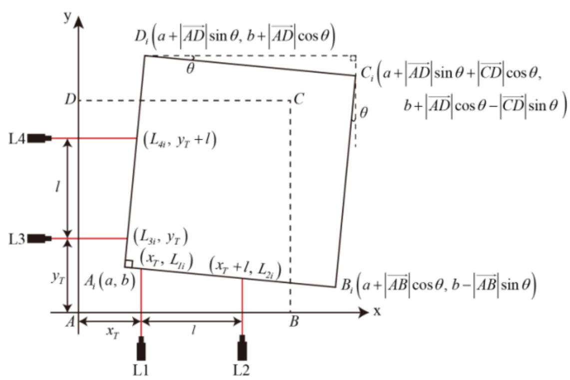

Fig. B1 Coordinate of edge point in torsional angle measurement using LDS

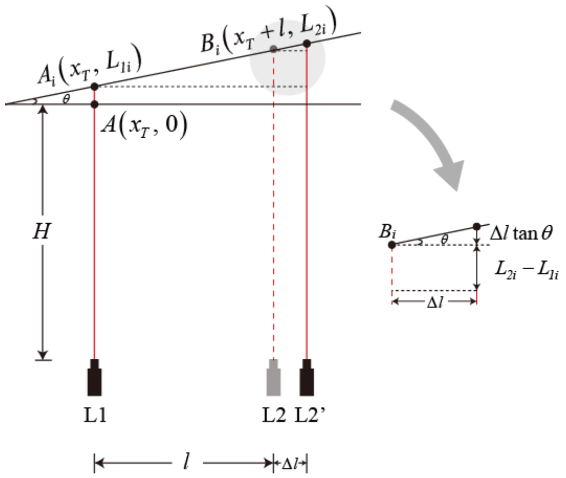

Fig. C1 Measurement error from distance between LDSs

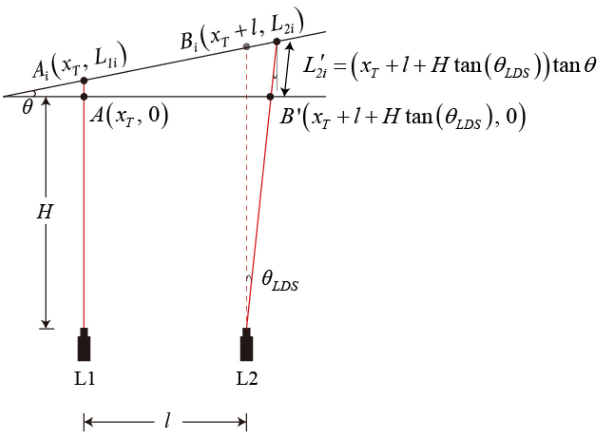

Fig. C2 Calculation of measurement error by θ_{LDS}

$$\theta = \cos^{-1}\left(\frac{\overrightarrow{AB}\cdot\overrightarrow{A_iB_i}}{\left|\overrightarrow{AB}\right|\left|\overrightarrow{A_iB_i}\right|}\right) = \cos^{-1}\left(\frac{l}{\sqrt{l^2+\left(\left(x_T+l+H\tan\left(\theta_{LDS}\right)\right)-L_{1i}\right)^2}}\right) \quad \text{(C3)}$$

$$\text{for}\left(x_T+l+H\tan\left(\theta_{LDS}\right)\right)-L_{1i}>0$$

$$\theta = -\cos^{-1}\left(\frac{\overrightarrow{AB}\cdot\overrightarrow{A_iB_i}}{\left|\overrightarrow{AB}\right|\left|\overrightarrow{A_iB_i}\right|}\right) = -\cos^{-1}\left(\frac{l}{\sqrt{l^2+\left(\left(x_T+l+H\tan\left(\theta_{LDS}\right)\right)-L_{1i}\right)^2}}\right) \quad \text{(C4)}$$

$$\text{for}\left(x_T+l+H\tan\left(\theta_{LDS}\right)\right)-L_{1i}<0$$

As such, to measure the structural torsional response that creates the pure translation and rotation using 4 LDSs, LDS must be installed precisely with regards to separation distance and perpendicular direction.